Lyotropic Phase Morphologies of Amphiphilic Block Copolymers

S. Förster*

Institut für Physikalische Chemie, Universität Hamburg, Bundesstrasse 45, D-20146 Hamburg, Germany

B. Berton, H.-P. Hentze, E. Krämer, and M. Antonietti

Max-Planck-Institut für Kolloid- und Grenzflächenforschung, Am Mühlenberg, D-14476 Golm, Germany

P. Lindner

Institut Laue-Langevin, Avenue des Martyrs, BP 156, F-38042 Grenoble Cedex 9, France

Received November 8, 2000; Revised Manuscript Received March 15, 2001

ABSTRACT: Lyotropic phase morphologies of amphiphilic poly(butadiene-*b*-ethylene oxide) (PB−PEO) block copolymers are studied using transmission electron microscopy, small-angle X-ray scattering, small-angle neutron scattering, and polarized optical microscopy. The PB−PEO block copolymers form type-1 lyotropic phases comprising disordered micellar solutions (L_1), spheres arranged on a bcc lattice (I_1), hexagonally packed cylinders (H_1), and lamellae (L_α). Increasing molecular weight destabilizes the I_1 and H_1 phases and lowers the degree of order. For high molecular weight block copolymers the increase in chain conformational entropy leads to the formation of the sponge phase (L_3). The transmission electron micrographs allow a detailed analysis of packing defects and epitaxial relations of the block copolymer lyotropic phases.

1. Introduction

Amphiphilic block copolymers consist of a hydrophobic polymer that is covalently linked to a hydrophilic polymer. They have the same structural characteristics as low molecular weight surfactants and lipids. In aqueous solutions, this leads to self-assembly into micellar structures and lyotropic phases. The principles governing self-assembly not only are interesting in their own right but also have considerable implications for materials science. Amphiphilic copolymers find numerous applications as emulsifiers, wetting agents, foam stabilizers, thickeners, rinse aids, and compatibilizers.[1] Recent years have seen considerable progress in using self-assembled polymeric structures for pharmaceutical applications,[2] and for the preparation of nanostructured materials such as semiconductors, nobel metals, and mesoporous ceramics.[3]

Motivated by the fascinating self-assembly behavior and potential applications of amphiphilic block copolymers, researchers have in recent years extensively studied lyotropic phase behavior. The most prominent systems have been triblock copolymers of the type poly(ethylene oxide-*b*-propylene oxide-*b*-ethylene oxide) ($E_mP_nE_m$) which are commercially available as Pluronics or Synperonics[4−7] and poly(ethylene oxide-*b*-butylene oxide-*b*-ethylene oxide) ($E_mB_nE_m$) triblock copolymers (Tetronics).[8−10] Phase diagrams have been published both for binary (polymer/water)[11] and ternary mixtures (polymer/water/oil),[12,13] and many analogies to the phase behavior of low molecular weight surfactants and bulk block copolymers have been established.

An important goal of such studies has been the identification of the major parameters that relate polymer structure and external variables (concentration, temperature, shear fields) to phase morphology. This has motivated the synthesis of well-defined amphiphilic block copolymers with narrow molecular weight distributions, controllable block lengths and high purity. Commercially available polyoxyalkylene block copolymers often contain diblock and homopolymer impurities and are quite polydisperse. Different batch-polymerization charges can have different properties which complicate a quantitative interpretation of experimental data with theoretical models. For example, in the case of "L122" ($E_{11}P_{70}E_{11}$), notably different phase diagrams have been reported by different laboratories.[11,14]

Using living anionic polymerization, model amphiphilic block copolymers such as poly(butylene oxide-*b*-ethylene oxide) (B_nE_m)[15] and several poly(olefin-*b*-ethylene oxide) block copolymers like poly(styrene-*b*-ethylene oxide) (PS−PEO), poly(butadiene-*b*-ethylene oxide) (PB−PEO), and poly(isoprene-*b*-ethylene oxide) (PI−PEO), together with their hydrogenated versions (PEE-PEO, PEP−PEO) have become available.[16−19] In the case of PS−PEO, block copolymers are only directly water-soluble below PS-molecular weights of 3000 where the glass-transition temperature, T_g, of PS is still below or around ambient temperature. The low glass-transition temperature of the PB-, PI-, PEE-, and PEP-hydrophobic blocks ($T_g < -20$ °C) renders these polymers water-soluble even at large hydrophobic block lengths. These block copolymers have been shown to be promising model systems for the investigations of block copolymer lyotropic phase behavior.[20]

The most common techniques that have been used for the structural analysis of polymer lyotropic phases are polarized optical microscopy (POM), small-angle X-ray scattering (SAXS), differential scanning calorimetry (DSC), and NMR. Transmission electron microscopy (TEM) is not routinely used, although much more detailed information on the structure and topology of lyotropic phases could be gained. In a preceding paper we have used TEM to study polymer lyotropic phases and mesoporous silicates prepared therefrom.[21] This

10.1021/ma001923h CCC: $20.00
Published on Web 05/19/2001

Table 1. Block Copolymer Degrees of Polymerization *N*, Polydispersity Index M_w/M_n, Volume Fraction of the PB-Block f_{PB}, and Polymer Density ρ of the Samples Investigated in the Present Study

sample-ID	N_{PB}	N_{EO}	M_w/M_n	f_{PB}	ρ
PB−PEO-8	202	360	1.06	0.476	1.020
PB−PEO-11	432	484	1.02	0.591	0.990
PB−PEO-12	797	893	1.04	0.591	0.990
PB−PEO-13	16	102	1.05	0.202	1.091
PB−PEO-14	125	155	1.02	0.566	0.996

became possible by covalently cross-linking the lyotropic phases of PB−PEO block copolymers using γ-irradiation. In the present paper we report a detailed study of lyotropic phase morphologies of different PB−PEO block copolymers using transmission electron microscopy (TEM), small-angle X-ray (SAXS) and small-angle neutron scattering (SANS), and polarized optical microscopy (POM). We particularly focus on a detailed structural characterization of different lyotropic phases, their domain boundaries, the effect of concentration and molecular weight on order and topology, and on major parameters that govern lyotropic phase behavior.

2. Experimental Part

Polymer Synthesis. Poly(butadiene-*b*-ethylene oxide) (PB−PEO) block copolymers were synthesized by sequential living anionic polymerization following a recently developed procedure.[16,19] It utilizes the phosphazene base *t*-BuP_4 to polymerize both butadiene and ethylene oxide with lithium as the counterion which allows one to synthesize PB−PEO by simply adding ethylene oxide to the living polybutadiene block ("one-pot−two-shot" procedure). *sec*-BuLi was used as the initiator and THF as the solvent. The reaction was quenched with acetic acid, and the block copolymers were precipitated in cold (−30 °C) acetone and dried under vacuum to constant weight.

Polymer Characterization. The molecular weight of the PB block was determined from a precursor drawn from the reaction solution prior to the cross-step to ethylene oxide. The precursor, after quenching with degassed methanol, was analyzed with GPC in $CHCl_3$, calibrated with polybutadiene standards (Polymer Standards Service). The molecular weight of the PEO block was determined from the peak ratios determined by ^{1}H NMR.[19] The characteristic molecular parameters are summarized in Table 1.

Polymer Solutions and Gels. Polymer solutions and gels were prepared by mixing the block copolymer with deionized water (Milli-Q water purification system) at a given weight fraction in 5 mL screw test tubes. The samples were homogenized by intense mechanical mixing, annealed at 60 °C for 24 h and further equilibrated at room temperature for 2 days. Lyotropic phases were cross-linked by exposing the samples to a ^{60}Co γ-radiation source for several days (dose rate: 55.67 krad/h).

Polarized Optical Microscopy. Optical textures of the lyotropic phases were investigated with a polarized optical microscope (Olympus BX50). Thin films of the lyotropic phases were prepared between a glass slide and a cover slide and sealed with silicon grease to avoid solvent evaporation.

Transmission Electron Microscopy. Lyotropic gels were dried using critical-point drying (BAL-TEC CPD 030) after stepwise exchange of water for acetone followed by a subsequent solvent exchange to supercritical CO_2. The dried samples were embedded in epoxy resin and microtomed using a Leica Ultracut UCT with a 45° diamond knife (Diatome). The thickness of the microtomed section varied between 30 and 50 nm. Transmission electron microscopy was performed with a Zeiss EM912 Omega TEM, operating at an acceleration voltage of 120 kV. The contrast of the samples was sufficiently high, so that no staining was necessary.

Small-Angle X-ray Scattering. Small-angle X-ray scattering (SAXS) measurements were performed on a setup consisting of a rotating anode (Nonius FR591, λ(Cu K_α) = 0.154 nm) and a home-built camera equipped with image plates. One-dimensional scattering curves were obtained by sector averaging. The scattering vector is defined as $s = (2/\lambda)\sin(\theta/2)$, where θ is the scattering angle. 2 mm thick clear bulk films were obtained by melt-pressing at 80 °C under vacuum.

Small-Angle Neutron Scattering. Small-angle neutron scattering (SANS) was performed at the 20.0 m detector position at the D11 small-angle instrument at ILL, Grenoble. The neutron wavelength was $\lambda = 0.6$ nm with $\Delta\lambda/\lambda = 8\%$ (from fwhm). Details of the instrumentation and data reduction can be found elsewhere.[22] 2 mm thick films of the gellike lyotropic phases in D_2O were sealed into Al-foil to avoid evaporation of solvent during the measurement. Bulk films were melt pressed as described above.

3. Results and Discussion

Transmission electron microscopy is one of the most direct ways to obtain structural information on lyotropic phases. In the case of low molecular weight lyotropic structures, freeze-fracture or freeze-etching electron microscopy (FFEM)[23] and cryo-electron microscopy (cryo-TEM)[24] have been successfully used. They have, however, not been applied for polymeric lyotropic phases.

A requirement for using TEM is a fixation of the lyotropic phase so that sample preparation and investigation under high vacuum do not alter its structure. Fixation can be achieved by chemically cross-linking the block copolymers in the lyotropic phase. Among the techniques for chemical cross-linking are alkylations,[25] photoreactions,[26−29] and the generation of macroradicals by redox reactions.[30] Radicals can also be generated by high energy (ionizing) radiation, in particular γ-irradiation. Radioisotope sources produce γ-rays with high penetration depths and are routinely used for the preservation of food, sterilization of medical devices, and cross-linking of high performance polymer composites.[31] ^{60}Co is one of the most common radiation sources for the commercial cross-linking of organic materials.

The mechanism of cross-linking of polymers with high energy (ionizing) radiation proceeds via macroradicals which react to lead to cross-linking and chain scission. The effect on the polymeric materials depends on the efficiency of the cross-linking reactions with respect to the main-chain scission efficiency. Polybutadiene has the highest cross-linking efficiency of all common polymers at negligible chain scission. Polyoxyalkylenes show about equal, but more than an order of magnitude lower cross-linking and scission efficiency.[31] According to the theory of Flory and Stockmayer,[32] the number of cross-link sites to reach the gelation threshold is inversely proportional to the molecular weight of the polymer chain. Accordingly, larger doses are needed to cross-link samples with lower molecular weight. We have found that cross-linking by γ-irradiation is particularly suitable for PB−PEO block copolymers. We have not been successful to cross-link commercially available PEO−PPO−PEO (Pluronic series, BASF), PS−PEO (SE-series, Th. Goldschmidt AG), or PEP−PEO (KLE-series, Th. Goldschmidt AG) block copolymers which have quite low molecular weights and consist of polymers with lower cross-linking efficiencies.

The transmission electron micrographs of the lyotropic phases allow the determination of the size and shape of the amphiphile aggregates (spheres, cylinders, vesicles, bilayers), the symmetry and size of the unit cell of the liquid crystalline phases (cubic, hexagonal, lamellar), and the identification of structural defects and epitaxial relations. These data allow one to calculate volume

fractions of microphases and the interfacial area per polymer chain, which are parameters that are expected to play a major role in the lyotropic phase behavior of block copolymers. These results are complemented by information gained from SAXS, SANS, and polarized optical microscopy (POM).

Samples were prepared by dissolving the polymer in water at a given polymer weight fraction w, from which the volume fraction of the hydrophobic PB domain, ϕ_{PB}, can be calculated and compared to the results obtained by electron microscopy. At a given weight fraction of polymer, the PB-volume fraction ϕ_{PB} is given by

$$\phi_{PB} = f_{PB,\nu} \frac{w}{w + (1 - w)\dfrac{\bar{\rho}_P}{\rho_W}} \tag{1}$$

where ρ_W is the density of water, $\bar{\rho}_P$ the density of the block copolymer, and $f_{PB,\nu}$ the volume fraction of PB in the block copolymer. $\bar{\rho}_P$ and $f_{PB,\nu}$ are given by the chemical structure of the block copolymer. They are calculated as $f_{PB,\nu} = \nu_{PB}/(\nu_{PB} + \nu_{PEO})$ and $\bar{\rho}_P = (m_{PB} + m_{PEO})/(\nu_{PB} + \nu_{PEO})$ where $\nu_i = N_i(M_i/\rho_{i_i}N_L)$ are the volumes and $m_i = N_i(M_i/N_L)$ the masses of the respective blocks (i = PB,PEO). The N_i are the degrees of polymerization, M_i are the monomer molecular weights, N_L is Avogadro's constant, and ρ_i are taken as the bulk densities of the respective homopolymers which are ρ_{PB} = 0.884 g/cm^3 [33] and ρ_{PEO} = 1.143 g/cm^3.[20,34]

The volume fraction ϕ_P can also be calculated from the electron micrographs through the measured radii R of the PB domains (sph = sphere, cyl = cylinder, lam = bilayer) and the unit cell dimension a as

$$\phi = \begin{cases} \dfrac{8\pi}{3}\dfrac{R_{sph}^{\,3}}{a^3} & \text{for } I_1 \ (bcc) \quad (d = 3) \\ \dfrac{2\pi}{\sqrt{3}}\dfrac{3R_{cyl}^{\,2}}{a^2} & \text{for } H_1 \qquad (d = 2) \\ \dfrac{2R_{lam}}{a} & \text{for } L_\alpha \qquad (d = 1) \end{cases} \tag{2}$$

d is the dimensionality of the domains, which is $d = 3$ for spheres, $d = 2$ for cylinders, and $d = 1$ for lamellae or bilayers. I_1 denotes a micellar cubic phase (bcc, space group $Im3m$), H_1 hexagonally packed cylinders, and L_α the lamellar phase. For L_α, R_{lam} is equal to half the thickness of the PB lamellae. Important thermodynamic parameters are the interfacial area of the PB/water interface per unit volume, A_V, which is given by

$$A_V = d\frac{\phi_{PB}}{R} \tag{3}$$

and the corresponding interfacial area per block copolymer chain, $\bar{a}$, which can be calculated as

$$\bar{a} = d\frac{N_{PB}\bar{\nu}_{PB}}{R} \tag{4}$$

where d is the dimensionality and R the radius of the PB domain.

The block copolymers in Table 1 form a variety of different normal (type-I) lyotropic phases. We will first discuss the sample $PB_{202}E_{360}$ (PB−PEO-8) which forms a common sequence of lyotropic phases $L_1 \rightarrow I_1 \rightarrow H_1 \rightarrow L_\alpha \rightarrow X$ with increasing concentration. L_1 denotes the disordered micellar phase and X the bulk (semicrystalline) phase. $PB_{125}E_{155}$ (PB−PEO-14) forms cylindrical micelles in dilute solutions which allows to study the ordering and packing of cylindrical micelles into a hexagonal liquid crystalline phase. Block copolymer molecular weights have a pronounced effect on the degree of order in a lyotropic phase. This effect is investigated with the high molecular weight samples $PB_{432}E_{484}$ (PB−PEO-11) and $PB_{797}E_{893}$ (PB−PEO-12). Characteristic parameters of the lyotropic phases are summarized in Table 2.

3.1. Lyotropic Phase Sequence of $PB_{202}E_{360}$ (PB−PEO-8). At room temperature there is the common sequence of type-I phases $L_1 \rightarrow I_1 \rightarrow H_1 \rightarrow L_\alpha \rightarrow X$. Representative electron microscopy images of the lyotropic phases are shown in Figure 1, parts a−e. A similar sequence of phases has been reported for $E_{27}P_{61}E_{27}$ ("P104"), a well-investigated polyoxyethylene block copolymer with similar block length ratio[11] (PEO_{27}−PPO_{61}−PEO_{27}), and also for low-molecular weight nonionic surfactants.[35,36]

At a volume fraction of ϕ_{PB} = 0.19 (w = 40%) we observe an ordered cubic micellar phase (I_1). The electron micrographs show dark PB-spheres arranged on a bcc lattice. The degree of order is quite high; single ordered domains extend to several μm. The micellar cores have a radius of R_{sph} = 21nm. The typical projections of a bcc lattice, i.e., the [100]- and [110] projections are indicated. Characteristic is the [100]-projection having a 4-fold symmetry axis with four dark spheres arranged on a square with a square sublattice of gray spheres representing the body-centered spheres in the unit cells. With a lattice constant of a = 77 nm and a sphere radius of 21 nm this corresponds to a volume fraction of ϕ_{PB}^{geo} = 0.17 in good agreement with the bulk volume fraction.

bcc lattices are expected for spheres with a soft repulsive potential ("soft spheres") as in the case of block copolymer micelles with large corona blocks where the intermicellar potential depends only logarithmically, i.e., $u(r) \sim \ln(l/r)$, on the distance between micelles.[37] For hard spheres an fcc lattice would be expected. The occurrence of fcc and bcc packing in micellar gels has been reported by McConnell et al.[38] who pointed out an important analogy to the structure of charged colloidal systems.[39,40] Generally, short-range repulsion favors fcc whereas long-range repulsion leads to bcc-packing. In the block copolymer phase diagram by Matsen and Bates there also is a narrow window of fcc between the disordered phase and the bcc phase.[41] Whether there is a narrow window of I_1(fcc) between the L_1 and I_1(bcc) phases for $PB_{202}E_{360}$ (PB−PEO-8) is a topic of ongoing investigations.

Increasing the volume fraction to ϕ_{PB} = 24 (w = 50%) leads to the formation of densely packed cylindrical micelles (Figure 1b). PB-cylinders have a radius of R_{cyl} = 19 nm. From the cylinder-to-cylinder distance a = 75 nm follows a volume fraction of ϕ_{PB}^{geo} = 0.21, assuming hexagonal cylindrical packing in good agreement with the bulk value. The unit cell dimension is indicated in Figure 1b. The degree of order is lower compared to the cubic phase. The differences in projected cylinder lengths in the TEM-micrographs indicate large variations of the cylinder direction (large director fluctuations).

Table 2. Polymer Weight Fraction w, PB-Volume Fraction ϕ_{PB}, Lyotropic Phase Morphology, Particle Radius R_c, Average Distance or Unit Cell Dimension a, Calculated PB-Volume Fraction ϕ_{PB}^{geo}(Eq 2), Interfacial Area/Volume A_V, and Area Per Chain $\bar{a}$ for the Samples Investigated in the Present Study

w	ϕ_{PB}	morphology	R_c (nm)	a (nm)	ϕ_{PB}^{geo}	A_V (nm^{-1})	$\bar{a}$ (nm^2)
			PB−PEO-8				
0.40	0.19	bcc spheres (I_1)	21	77	0.17	0.024	3.0
0.50	0.24	cylinders	19	75	0.21	0.025	2.2
0.60	0.28	cylinders	15	73	0.25	0.026	5.4
		ribbons				0.025	
		vesicles					
0.70	0.33	cylinders	20	66	0.36		
		platelets	9				
		vesicles					
0.80	0.38	lamellae (L_α)	9	47	0.38	0.042	2.3
1.00	0.48	lamellae (L_α)	9	38	0.47	0.053	2.3
			PB−PEO-11				
0.30	0.18	spheres (L_1)	31	112	0.18	0.017	4.3
0.50	0.30	hex cylinders (H_1)	29	105	0.28	0.019	3.1
0.70	0.42	lamellae (L_α)	15	74	0.41	0.027	3.0
1.00	0.59	lamellae (L_α)	15	52	0.58	0.038	3.0
			PB−PEO-12				
0.30	0.178	spheres (L_1)	51			0.010	4.9
		cylinders					
0.50	0.297	sponge (L_3)	47	160		0.010	3.5
0.70	0.415	lamellae (L_α)	32	161	0.40	0.012	2.6
1.00	0.591	lamellae (L_α)	30	102		0.027	2.7
			PB−PEO-14				
0.001	0.0006	cylinders	(17)			0.000 06	2.28
0.02	0.01	cylinders				0.0011	
0.30	0.17	hex cylinders (H_1)	13	47	0.28	0.043	1.99
0.50	0.28	hex cylinders (H_1)	13	43	0.33	0.051	1.99
0.60	0.34	hex cylinders (H_1)	13	45	0.30	0.047	
		lamellae (L_α)					
0.70	0.40	lamellae (L_α)	6.6	34	0.39	0.059	1.96
1.00	0.57	lamellae (L_α)	6.6	23	0.57	0.086	1.96

There is a broad coexistence region of H_1 and L_α for $0.25 \leq \phi_{PB} \leq 0.35$(45 < w < 75%). This appears to be a general characteristic of block copolymer lyotropic phases and is also observed for $PB_{125}E_{155}$ (PB−PEO-14) and for many Pluronic systems such as $E_{27}P_{61}E_{27}$ ("P104").[11] In Figure 1c,d we observe cylinders with radii $R_{cyl} = 19$ nm in coexistence with small bilayer platelets having lateral dimensions between 0.5 and 1 μm. Bilayers and cylinders seem almost homogeneously mixed. Extended coexisting pure H_1 and L_α domains are not observed throughout the whole sample. Locally, stacks of bilayers terminate at rows of cylinders that are arranged normal to the bilayers (see Figure 2). This seems to be a relatively stable domain boundary. As the coexistence region between H_1 and L_α is quite large, the free energy difference between a disklike and a cylindrical state seem quite small. As expected, at $\phi_{PB} = 0.28$ ($w = 60\%$) the fraction of cylinders is larger than at $\theta = 0.33$ ($w = 70\%$) (Figure 1d). Similar to cylindrical micelles that have spherical caps, we observe the disklike bilayers to have cylindrical rims.

At $\phi_{PB} = 0.38$ ($w = 80\%$) only the lamellar phase (L_α) is stable. The lamellae thickness is $2R_c = 18$ nm corresponding roughly to the $R_{lam} = R_{cyl}/2$ relation expected from packing considerations. In bulk ($\phi_{PB} = 0.48$) we observe a lamellar structure as in all bulk PB−PEO samples due to crystallization of the PEO block.

3.2. Ordering and Epitaxy of PB_{125}-E_{155} (PB−PEO-14). Compared to $PB_{202}E_{360}$ (PB−PEO-8), this block copolymer has a larger hydrophobic fraction and a shorter soluble block which tends to stabilize the cylindrical phase as is the case for $E_{20}P_{70}E_{20}$ ("P123").[11] It shows a sequence of phases: $L_1 \rightarrow H_1 \rightarrow L_\alpha \rightarrow X$, where the micelles in the dilute micellar phase L_1 have a cylindrical shape. Electron micrographs of micellar and lyotropic structures are shown in Figure 3, parts a−f.

At $\phi_{PB} = 0.001$ ($w = 0.1\%$) the block copolymer forms cylindrical micelles with an overall radius (core + shell) of $R = 13$ nm. Cylindrical micelles have contour lengths of several μm. Occasionally the cylinders form loops and cross-links. The end-caps have a larger radius $R_{cap} = 25$ nm which roughly corresponds to the ratio of packing parameters $R_{cyl} \approx 2R_{sph}/3$. According to Israelachvili[42] this limit is expected for infinitely long cylinders. Cylindrical or wormlike micelles of low molecular weight surfactants have interesting thermodynamic and rheological properties.[43] Detailed structural studies of polymeric wormlike micelles in aqueous solution have recently been reported for (PEE_{45}−E_{55})[30] and for PEO_{45}−PIB_{37}−PEO_{45} using cryo-electron microscopy.[44]

At higher volume fractions, $\phi_{PB} = 0.01$ ($w = 2\%$) we observe wormlike micelles to form an isotropic entangled network structure which is structurally equivalent to the transient network of linear polymer chains above the overlap concentration c^* in the semidilute solution regime.[45] The average mesh size is $\xi \approx 150$ nm. The transition from the dilute to semidilute solution regime for wormlike micelles of the low molecular weight nonionic surfactant $C_{16}E_6$ has recently been inferred from scattering experiments by Schurtenberger et al.[46]

It is expected that rodlike micelles form nematic phases (N_1) above a certain concentration.[47] A nematic phase for (PEE_{45}−E_{55}) in the concentration range $15 \leq w \leq 20\%$ has been recently reported between the isotropic L_1 phase and the hexagonal H_1 phase.[30] However, for PB_{125}−E_{155} (PB−PEO-14) we observe a

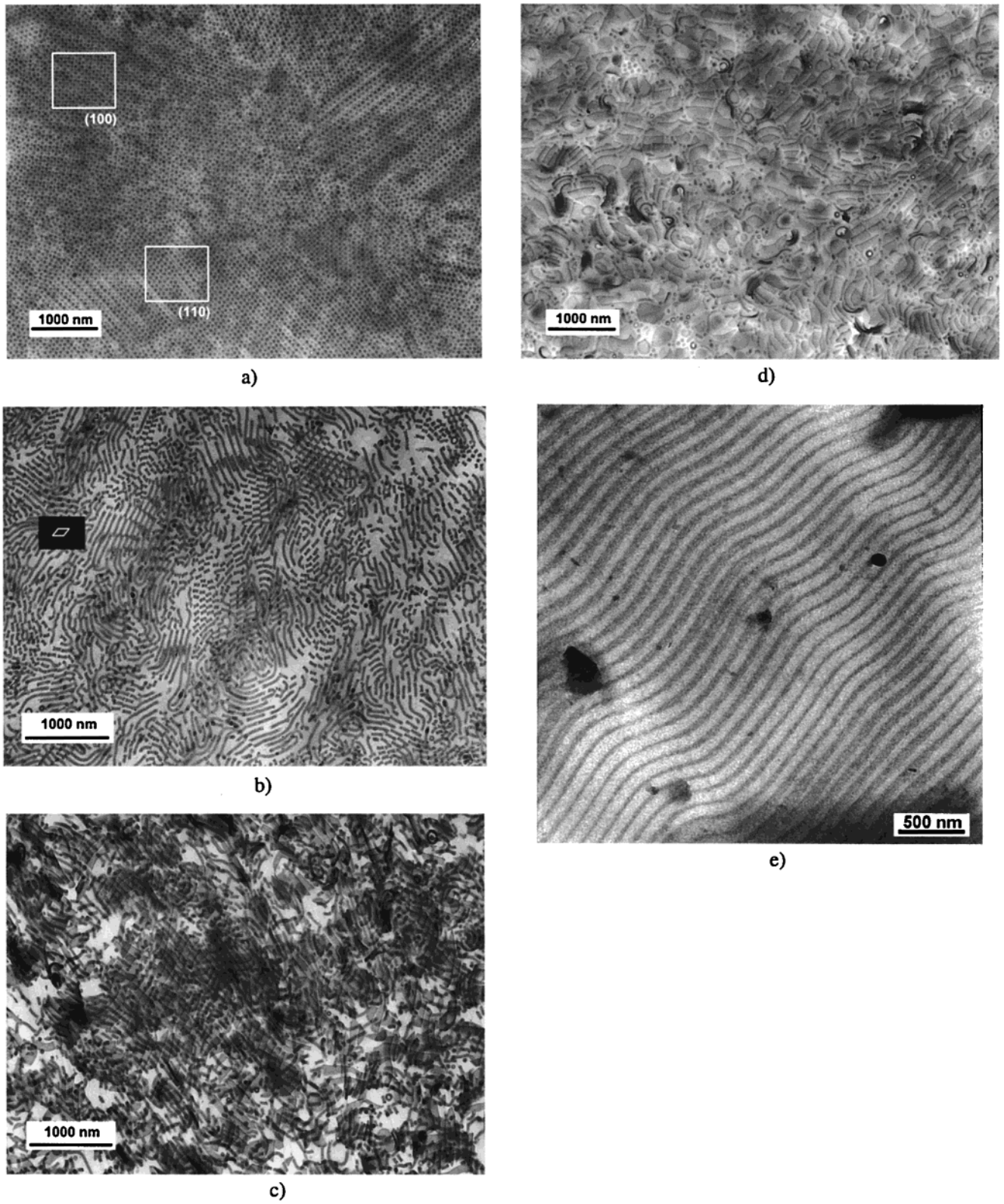

Figure 1. Electron micrographs of lyotropic liquid crystalline phases of sample PB−PEO-8 at polymer weight fractions $w = 0.40$ (I_1, bcc) (a), $w = 0.50$ (b), $w = 0.60$ (c), and $w = 0.70$ (d), and $w = 0.80$ (e). Different projections of the bcc lattice are indicated. The inset in part b indicates the hexagonal unit cell dimension.

somewhat different behavior. Over a broad concentration range of $0.02 < \phi_{PB} < 0.2$ ($4 < w < 35\%$) there is a coexistence of a dilute disordered L_1 phase and a more concentrated, ordered H_1 phase. Within this biphasic region the samples exhibit a pronounced turbidity. At $\phi_{PB} = 17$ ($w = 30\%$) the cylinder spacing determined from the electron micrographs in the H_1 domains is $a = 47$ nm which corresponds to a local volume fraction of $\phi_{PB}^{geo} = 30$ ($w = 55\%$) in the H_1 domains over nearly the whole biphasic concentration range. The coexistence

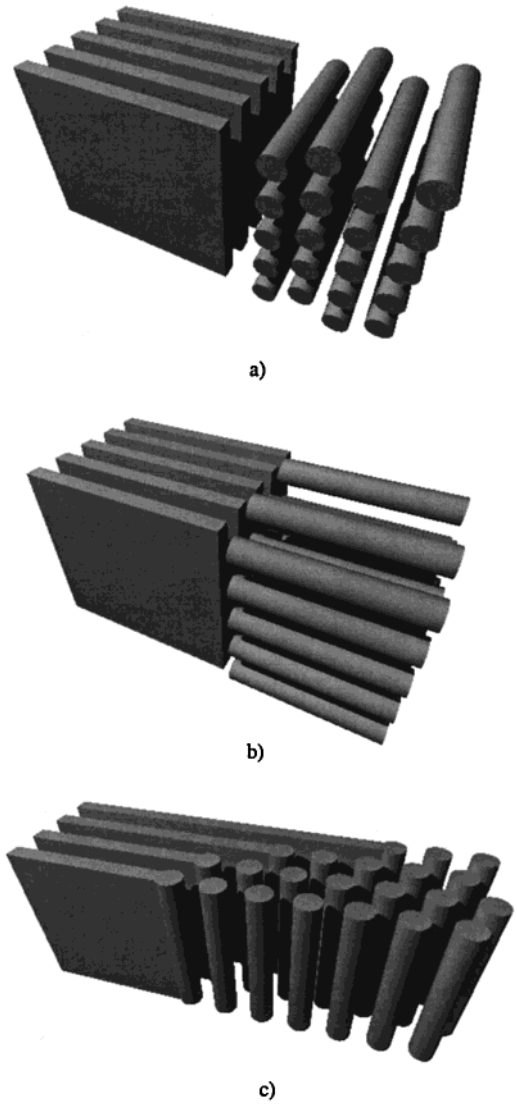

Figure 2. Schematic representation of three possible orientations at domain boundaries between H_1 and L_α domains. Cylinders oriented parallel to the plane normal (a), in-plane end-on (b), and in-plane, side-on (c). In domains with low degree of order, orientations a and b seem to be preferred, representing stable domain boundaries.

of ordered and disordered domains is clearly visible in Figure 3c.

Lyotropic liquid crystals can exhibit characteristic textures in polarized optical microscopy. One difficulty with block copolymer lyotropic phases is the preparation of samples with large uniformly oriented domains. These should have dimensions of at least several μm to obtain textures that can be visualized by polarized light microscopy. In the present study, samples of lyotropic H_1 phase of $PB_{125}-E_{155}$ (PB−PEO-14) at ϕ_{PB} ($w = 20\%$) were placed between a glass slide and a cover glass, sealed with silicon grease, and equilibrated for three months. The micrographs in Figure 4 are taken between crossed polarizers together with a λ/4-plate. Figure 4a shows "parallel striations" that correspond to the "fan-texture" typical for the H_1 phase. Figure 4b shows a "Maltese cross" formed by the striations. The λ/4-plate allows to see the striations in each of the four areas that converge at the center of the cross.

Similarly well-developed textures of high molecular weight block copolymers have only recently been reported by Wang and Hashimoto[48] for a PS−PI (M_n = 19 600). For lower molecular weight block copolymers, H_1 phase textures with "parallel striations" (E_{19}-$PDMS_{16}E_{19}$[49]), "fan-textures" ($E_{13}P_{30}E_{13}$ or "PE6400", Wanka et al.[11]), and "focal-conics" have been reported[50] as well as typical textures of L_α phases such as "oily streaks",[11,49] "polygonal arrays",[49] or fan-shaped Maltese crosses.[48]

Optical textures are directly related to certain packing defects (singularities, disclinations). Typical defects observed for the H_1 phase of $PB_{125}-E_{155}$ (PB−PEO-14) are shown in Figure 3c. We observe $k = +1/2$-disclinations where a cylinder after the 2π-turn reorients into the hexagonal array.There are also $k = -1/2$ type disclinations as indicated in Figure 3c. These defects are well-known from nematic phases. Localized on a line (singular line), they cause the striations observed in polarized optical microscopy.

Upon further increasing the polymer concentrations a coexistence of hexagonal and lamellar microdomains is observed. Figure 3d shows a well-defined orientation between the H_1 and L_α lattices. This orientation, with the hexagonal phase (10) planes parallel to the lamellar phase (001) planes, corresponds to the rows of cylinders oriented coplanar to the lamellae, as schematically shown in Figure 2c. The (001)-plane of L_α and (10)-plane of H_1 are the planes of highest density in each of the phases. It appears that the spatial alignment of a phase is dictated by the orientation of the phase from which it is derived (epitaxy). The cylinder next to the bilayer fuses to extend the bilayer in the direction of the row and vice versa. An arrangement of cylinders and bilayers such as in Figure 2, parts a and b, opposes such a fusion of cylinders into the adjacent bilayer. If the cylinders are opposite to the bilayer fuse, the bilayer−bilayer defect may be bridged by the formation of the Scherk-surface. It is a minimal surface with zero mean curvature that has been identified in lamellar block copolymer phases.[51] The repeat spacings of the H_1 and L_α lattices are observed to be commensurate, in the ratios $a_L/a_H = \sqrt{3}/2 \approx 0.87$. Such epitaxial relationships between lyotropic liquid-crystalline mesophases have been frequently observed, e.g., in a sequence such as $H_1-Q_1-L_\alpha$ where the repeat spacings of the planes were $a_{10}(H_1) = a_{211}(Q_1) = a_{001}(L_\alpha)$. Also the volume fractions ϕ_{PB} of both phases, calculated from the cylinder and lamellar thickness together with the lattice constants, are observed to be equal.

At $\phi_{PB} = 0.40$ ($w = 70\%$) only the lamellar phase (L_α) is stable. Images at low magnification show that space is completely filled with large multilamellar vesicles ("onions") with diameters of about 1 μm. The spontaneous curvature of the PB−PEO bilayers appears to be nonzero, leading to considerable bending of the lamellae to form vesicles. It has been shown that multilamellar vesicles or onions are topological defects of smallest energy for a given volume.[52] Such defects of positive Gaussian curvature are frequently observed for low molecular weight lyotropic surfactants. The observed multilamellar vesicles form spontaneously under quiescent conditions in contrast to shear-induced formation of multilamellar vesicles for the $E_{20}P_{70}E_{20}$ ("P123")/water/butanol system that has recently been reported by Zipfel et al.[53]

In the range of PB−PEO-molecular weights investigated in the present study there are no indications of an ordered bicontinuous cubic phase as is often observed between H_1 and L_α for lyotropic phases of low molecular

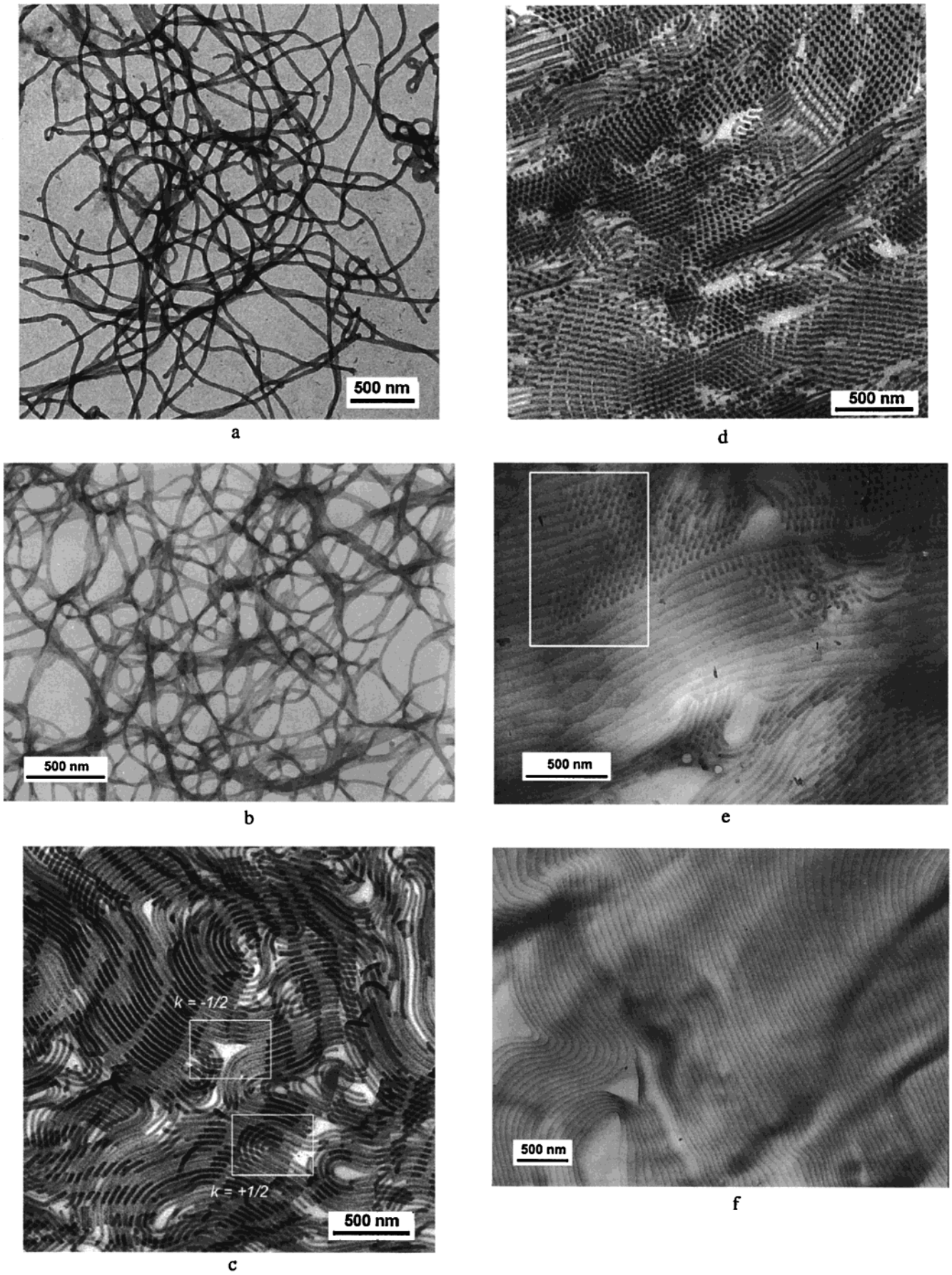

Figure 3. Electron micrographs of lyotropic liquid crystalline phases of sample PB−PEO-14 at polymer weight fractions $w = 0.001$ (a), $w = 0.02$ (b), $w = 0.50$ (H_1) (c), (d), $w = 0.60$ (H_1/L_α) (e), and $w = 0.70$ (L_α) (f). $k = +1/2$ and $k = -1/2$ disclinations are indicated in part c. There is a clear epitaxial relation in the H_1/L_α coexistence regime (part e).

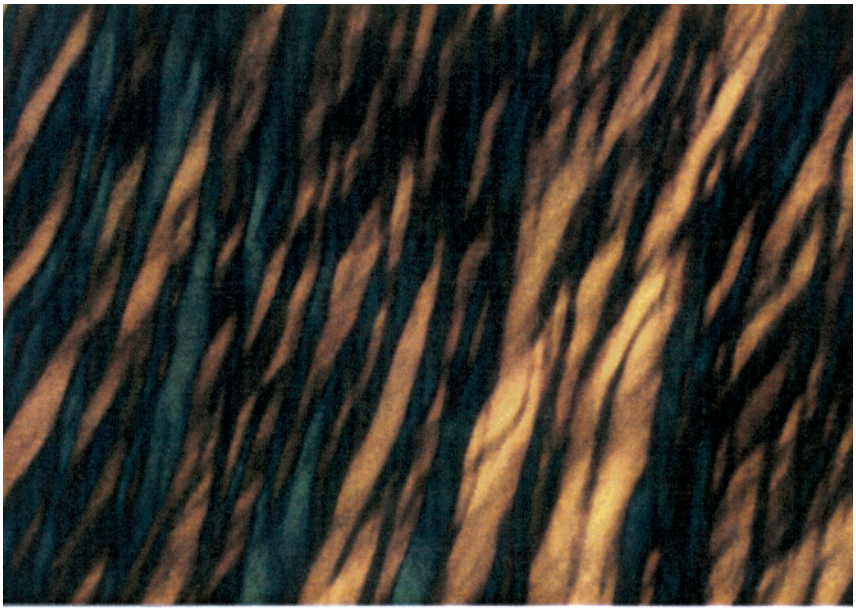

a

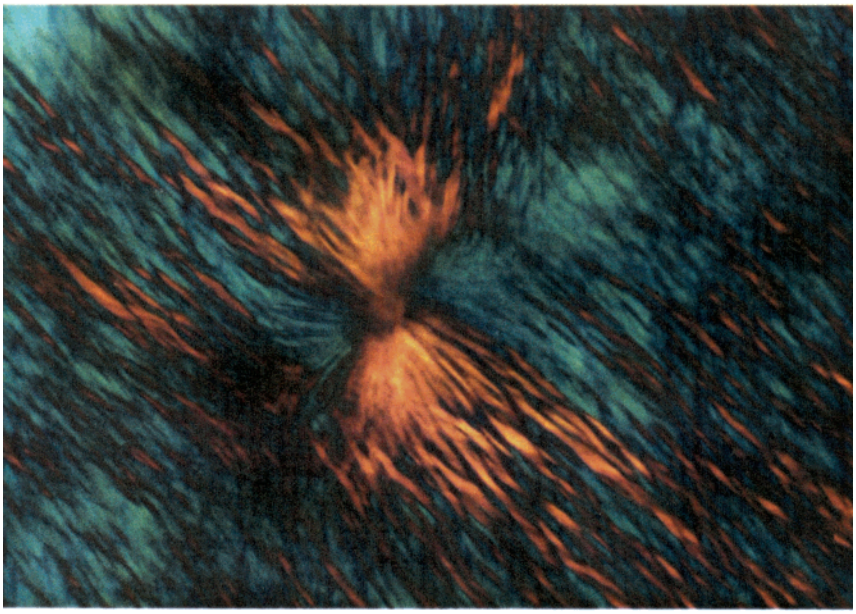

b

Figure 4. Typical optical textures of the H_1 phase ($w = 0.40$) observed between crossed polarizers with a quarter-wave plate: (a) "striations" and (b) "Maltese cross" consisting of striations. The striations correspond to the fan-texture of hexagonal liquid crystalline phases.

weight surfactants. The system PB−PEO/water is thermodynamically in the strong segregation limit ($\chi \approx 10$, $\chi N > 100$) where bicontinuous intermediate phases are unstable against hexagonal or lamellar phases.[41] At lower molecular weights bicontinuous cubic phases should become stable.

3.3. Conformational Entropy, Disorder, and L_3 Phases. It is expected and there is strong experimental evidence that with decreasing molecular weight the lyotropic phase behavior of amphiphilic block copolymers will eventually merge with the phase behavior of low molecular weight surfactants.[54] However, it is unclear whether there is any effect on the phase behavior if block copolymer molecular weights are progressively increased. This phenomenon is investigated with the samples $PB_{423}E_{484}$ (PB−PEO-11) and $PB_{797}E_{893}$ (PB−PEO-12).

Figure 5 shows electron micrographs of lyotropic phases of $PB_{423}E_{484}$ (PB−PEO-11). The molecular weight of this block copolymer is considerably larger compared to $PB_{125}E_{155}$ (PB−PEO-14) or $PB_{202}E_{360}$ (PB−PEO-8). Until quite large volume fractions we observe a disordered micellar phase (L_1), where at similar volume fractions the lower molecular weight samples developed well ordered cubic or hexagonal phases. At ϕ_{PB} ($w =$ 30%, Figure 5a) we observe spheres of radius $R_{sph} =$ nm arranged in a liquidlike order. At a higher volume fraction of $\phi_{PB} = 0.29$ ($w = 50\%$, Figure 5b) we observe disordered cylinders of radius $R_c = 29$ nm forming a mesh-like entangled network. At a volume fraction of

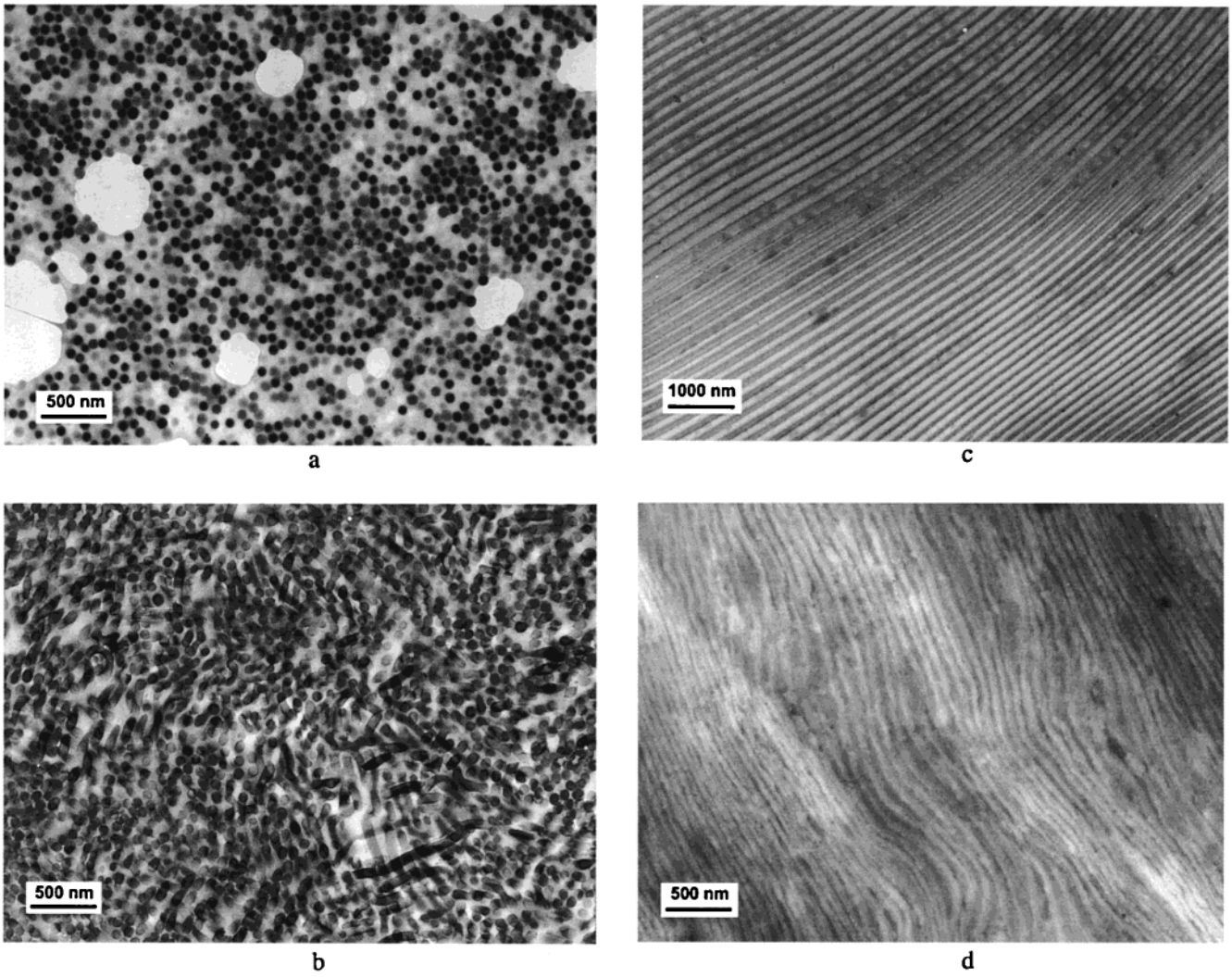

Figure 5. Electron micrographs of lyotropic liquid crystalline phases of sample PB−PEO-11 at polymer weight fractions w = 0.30 (a), w = 0.50 (b), w = 0.70 (c), and w = 1.0 (d). The degree of order is much lower compared to the lower molecular weight samples.

ϕ_{PB} = 0.41 (w = 70%, Figure 5c), we observe a well-ordered lamellar phase. It appears that the high molecular weight sample $PB_{423}E_{484}$ (PB−PEO-11) develops long-range order only at high concentrations.

Ordering on length scales larger than 100 nm can be followed with small-angle neutron scattering (SANS). The radially averaged scattering curves of $PB_{423}E_{484}$ (PB−PEO-11) at several volume fractions in D_2O are shown in Figure 6. The 2D-scattering patterns of all samples were isotropic, showing a diffraction ring at a scattering vector q^*, from which the average distance a between particles was calculated as $a = 2\pi/q^*$. The variation of a as a function of the volume fraction ϕ_{PB} is shown in the inset in Figure 6. Above a volume fraction of $\phi_{PB} > 0.2$, we observe a linear $a \sim \phi^{-1}$ dependence which is typical for lamellar phases. The volume fractions calculated from the characteristic distances of a = 112, 105, and 74 nm and the measured radii are in good agreement with values calculated from the weight fractions indicating homogeneous, single phase lyotropic solutions. The long period of the bulk L_α phase as measured by SANS is a = 52 nm, from which a lamellar thickness of R_c = 15 nm can be calculated from the PB-volume fraction $\phi_{PB} = f_{PB,v}$ = 0.59. From microtomed sections where the thickness is smaller than the domain period, it is often very difficult to directly deduce the lamellar thickness, particularly if the section is cut at oblique angles which is quite often the case.

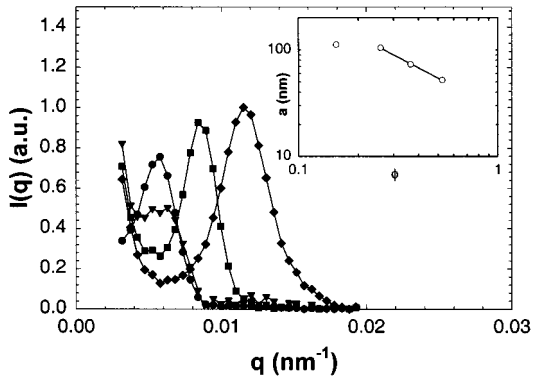

Figure 6. SANS-scattering curves for lyotropic phases of sample PB−PEO-11 at polymer weight fractions w = 0.30 (●), w = 0.50 (▼), w = 0.70 (■), and w = 1.00 (♦). The insert shows the $d \sim \phi^{-1}$ relation expected for the lamellar phase region.

For $PB_{797}E_{893}$ (PB−PEO-12), the largest of the block copolymers in the present study, lyotropic phases are even more disordered. At a volume fraction of ϕ_{PB} = 0.18 (w = 30%, Figure 7a) there is a pronounced polymorphism of micellar structures. We observe a coexistence

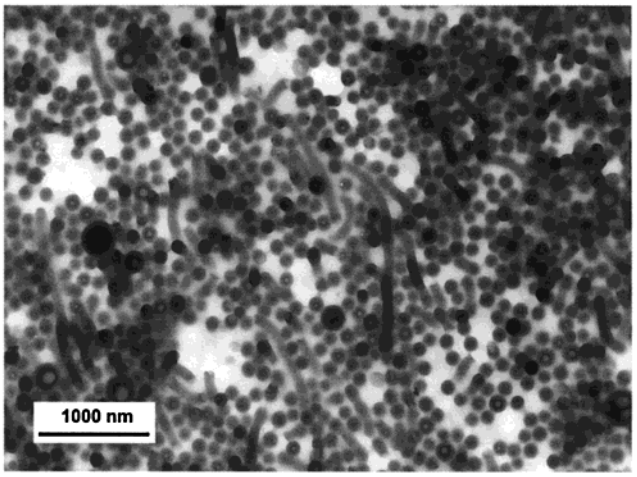

Figure 7. Electron micrographs of lyotropic liquid crystalline phases of sample PB−PEO-12 at polymer weight fractions $w = 0.30$ (a), $w = 0.50$ (b), and $w = 0.70$ (c). The appearance of the L_3 or sponge phase between L_1 and L_α is similar to phase sequences in microemulsions. There are small holes in the bilayers of the L_3 phase as indicated by the arrow.

of spherical micelles of radius $R_c = 51$ nm, wormlike micelles with the same radius, and small vesicles with overall radii between 57 and 100 nm. The vesicle interior domain has diameters between 25 and 100 nm. The unusually large bilayer curvature indicates the

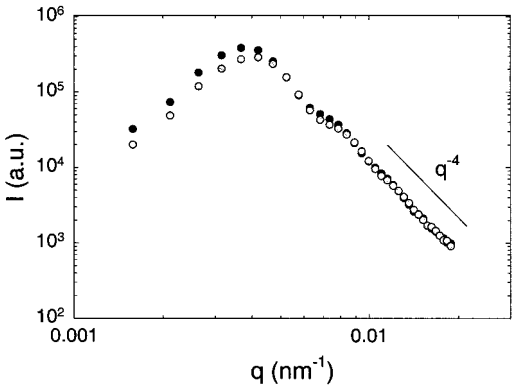

Figure 8. SANS curves of PB−PEO-12 at $w = 0.30$ (●) and $w = 0.40$ (gray circle) in the L_3 phase. There is a broad peak at $q \approx 0.004$ nm^{-1} related to the average distance or correlation length ξ between bilayers and a characteristic q^{-4}-scattering (Porod law) at high q due to scattering of the bilayer surface.

packing constraints play a minor role and only prevent vesicles from shrinking much below a certain critical packing radius. The system forms vesicles that are as small as possible with the lowest possible aggregation number to increase translational entropy.

At $\phi_{PB} = 0.30$ ($w = 50\%$), we observe a multiply connected, bicontinuous disordered phase that structurally corresponds to the L_3 phase or "sponge" phase (Figure 7b). It is built-up from PB-tripods and -tetrapods that are linked in a random fashion much like in a molten cubic bicontinuous phase. The L_3 phase shows no long-range order, but a well-defined characteristic length $\xi = 160$ nm which is related to an average unit cell size. The average radius of an elementary connecting passage is $R = 47$ nm. In μ-emulsions, the L_3 phase is found in phase diagrams close to the domain of the swollen lamellar phase L_α. On a local scale, the L_3 phase consists of the same bilayers as the swollen L_α phase. In surfactant systems, the structure of the L_3 phase was deduced from small-angle neutron scattering and measured transport properties.[55,56] Support for the proposed structure came from subsequent FFEM-studies.[57−59] For block copolymers, the L_3 phase has been observed for $E_{13}P_{30}E_{13}$ ("PE6200")[60] with a sequence of $L_1 \rightarrow L_\alpha \rightarrow L_3 \rightarrow L_2$, and recently for ternary A/B/AB-homopolymer/block copolymer mixtures[61,62] upon increase in temperature.

The SANS curve (Figure 8a) at a concentration of ϕ_{PB} ($w = 30\%$) exhibits a broad peak at $q^* = 0.038$ nm^{-1} corresponding to a characteristic length of $\xi = 2\pi/q^* = 165$ nm close to the characteristic length deduced from the TEM-images. At $\phi_{PB} = 0.24$ (40%) the peak shifts to $q^* = 0.042$ nm^{-1} corresponding to a length $\xi = 150$ nm. The SANS curves exhibit a weak shoulder at $q \approx 0.08$ nm^{-1} and a q^{-4}-decay (Porod law) at large scattering vectors due to scattering from the bilayer surface. These are typical features known also for L_3 phases formed by low-molecular weight surfactants.

An unusual feature of the L_3 phase is the presence of small holes in the bilayers, indicated by an arrow in Figure 7b. The holes have diameters of 20 nm which corresponds to the inner diameter of the vesicles observed at lower concentrations (Figure 7a). The presence of such holes was proposed in recent dielectric studies where unexpectedly large conductivities were observed for L_3 phases.[63−65] The fact that bilayer holes are similar in the L_3 phase and in vesicles also indicates the route on which the L_3 phase disconnects with decreasing

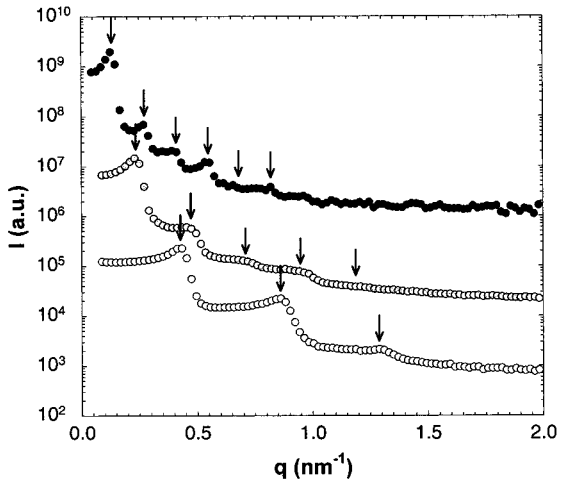

Figure 9. SAXS-scattering curves of lamellar bulk films of samples PB−PEO-13 (○), PB−PEO-14 (gray circle), and PB−PEO-11 (●). Arrows indicate the positions of the [*n*00] reflections.

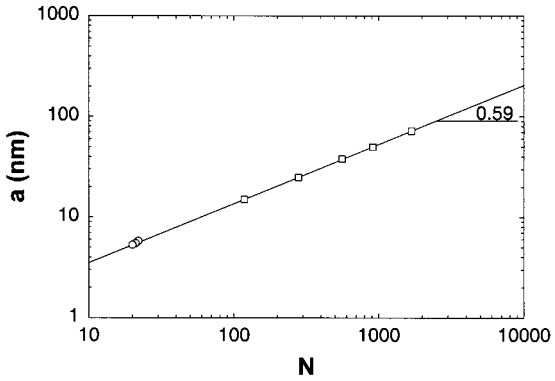

Figure 10. Lamellar long period *d* as a function of the total degree of polymerization of the block copolymers PB−PEO-8,11,12,13: (□). Also shown are data for low molecular weight $C_{12}E_y$-surfactants ($y = 5 - 10$) (○). The straight line is a linear regression of the data points to the relation $a = a_0 N^{\gamma}$ with $a_0 = 0.91$ nm and $\gamma = 0.59$. The value of the exponent is close to the value of $\gamma = {}^3/_5$ expected for the strong segregation limit (SSL).

concentration. According to theoretical predications, first a statistical distribution of holes is spontaneously formed in the L_3-bilayer. At lower concentrations, the number and average size of the holes increase so that the infinite multiconnected bilayer progressively disconnects into a dispersion of vesicles and micelles.[59]

At volume fractions of $\phi_{PB} = 0.41$ ($w = 70\%$), we observe lamellar domains with repeat distances of $a = 161$ nm together with large disordered domains containing bilayers and vesicles. The thickness of the lamellae is 64 nm. It is expected that the $L_\alpha \rightarrow L_3$ transition occurs when the interlamellar distance roughly equals the persistence length (or de Gennes−Taupin length) of the bilayer: i.e., $d > \xi$. It is difficult to determine the persistence length or bending radius from the electron micrographs, but from Figure 7c a bending radius of the bilayer of the order of 180 nm may be estimated. Upon diluting the L_α phase to $\phi_{PB} = 0.30$, the lamellar domain spacing would increase to $a = 250$ nm. This would represent a highly swollen lamellar phase with a domain spacing that is larger than the bilayer persistence length and therefore a transition to the L_3 phase would indeed be expected. $PB_{797}E_{893}$ (PB−PEO-12) shows the same sequence of phases, i.e., $L_1 \rightarrow L_3 \rightarrow L_\alpha$ as highly swollen surfactant systems. It appears that high molecular weight block copolymer lyotropic phases resemble microemulsions in the sense that large polymer blocks dilute the systems in a similar way as the addition of solvent (water or oil).

3.4. Bulk Phases. In bulk all PB−PEO samples form lamellar phases. Figure 9 shows the measured SAXS curves for $PB_{16}E_{102}$ (PB−PEO-13), $PB_{125}E_{155}$ (PB−PEO-14), and $PB_{432}E_{484}$ (PB−PEO-11). A set of [*n*00] reflections up to fifth order are observed indicating the formation of well-ordered lamellar phases.

From the positions of the reflections one obtains the lamellar long period *a*. In Figure 10 these are shown as a function of the degree of polymerization *N* for the block copolymers $PB_{16}E_{102}$ (PB−PEO-13), $PB_{125}E_{155}$ (PB−PEO-14), $PB_{202}E_{360}$ (PB−PEO-8), $PB_{432}E_{484}$ (PB−PEO-11), and $PB_{797}E_{893}$ (PB−PEO-12). Also included are long periods of lamellar phases formed by low molecular weight nonionic surfactants $C_{12}E_{5-10}$. These had been absorbed on graphite and imaged by AFM.[66] According to Semenov[67] there should be a relation $a \sim N^{2/3}$ in the strong segregation limit (SSL). This is fairly well fulfilled as shown by the straight line in Figure 10, which is a linear regression of the data to a $a = a_0 N^{\gamma}$ yielding $a_0 = 0.91$ nm and $\gamma = 0.59$ over 2 orders of magnitude in *N* including the surfactant data.

It is interesting to note that even a very asymmetric block copolymer such as $PB_{16}E_{102}$ (PB−PEO-13) which has a volume fraction of PB of only $\phi_{PB} = 0.13$ exhibits a lamellar phase. This has been attributed to crystallization of the PEO block. The tendency of the PEO block to crystallize thereby forming a lamellar phase has been reported for many systems including lyotropic phases of amphiphilic block copolymers, e.g. PEP−PEO,[20] $E_{90}B_{10}$ ($w \geq 70\%$),[68] and $E_{25}P_{40}E_{25}$ ("P85"),[69] and low-molecular weight amphiphiles, e.g. $C_{11}E_{40}$, $C_{15}E_{39}$, $C_{17}E_{40}$ ($w \geq 60\%$).[70,71]

3.5. Main Parameters Governing Phase Behavior. The self-assembly of block copolymers into lyotropic phases exhibits many features known from low-molecular weight amphiphiles and from bulk block copolymers. Recent advances in self-consistent field theory (SCFT) permit the calculation of binary and ternary phase diagrams of block copolymers in solution.[72] In the following, we briefly discuss some basic parameters like the interfacial area per chain and the interfacial area per volume and their relation to the observed phase behavior.

In the case of low-molecular weight amphiphiles, self-assembly can be described in terms of the surfactant packing parameter as introduced by Ninham and Israelachvili.[42] Within this framework, the structure of an amphiphile or surfactant is parametrized as $v/\bar{a}l$, where $\bar{a}$ is the area per headgroup, *l* is roughly equal to the fully extended length of the hydrocarbon chain, and *v* is the volume occupied by the surfactant. The packing parameter gives a critical condition below which certain micellar shapes are stable, i.e.

$$\frac{v}{\bar{a}l} < \begin{cases} 1/3, & \text{for spherical micelles} \\ 1/2, & \text{for cylindrical micelles} \\ 1, & \text{for bilayers} \end{cases} \qquad (5)$$

Entropy favors the smallest possible aggregate structures that are compatible with the packing parameter. For a given aggregate, the area per headgroup, $\bar{a}$, will be close to the optimum area $\bar{a}_0$, which is given by a balance of interfacial energy and headgroup repulsion.

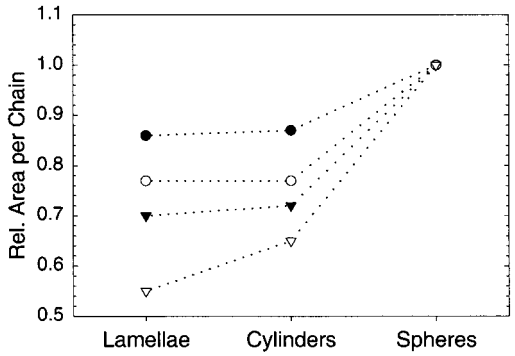

Figure 11. Variation of the area per chain $\bar{a}$ upon transitions from spherical to cylindrical to lamellar geometry for different polymer samples: PB−PEO-8 (○), PB−PEO-11 (▼), PB−PEO-12 (▽), and PB−PEO-14 (●). $\bar{a}$ values are normalized to the value for spherical geometry. For short-chain surfactants the area per chain would be nearly constant. The observed decrease with increasing molecular weight seems to be an effect of chain entropy.

It is a local property which should be independent of the total amphiphile concentration. Increasing temperature tends to decrease $\bar{a}$ in the case of nonionic surfactants, so that transitions form spherical to cylindrical or lamellar morphologies are observed. Assuming v and $\bar{a}$ to be constant for a given surfactant, and taking the radii to be equal to $R = l$, the radii of the aggregate structures should follow the relation

$$R_{\mathrm{sph}} = \frac{3}{2}R_{\mathrm{cyl}} = 3R_{\mathrm{lam}} \tag{6}$$

For a given surfactant the radii of spherical micelles, R_{sph}, should be larger than the radii of cylindrical micelles, R_{cyl}, which themselves should be larger than the radii of lamellae, R_{lam}. From Table 2, we observe that aggregate structures of PB−PEO indeed follow this trend.

We also observe some characteristic trends for the volume fractions of the phase transitions bcc (I_1) → HEX (H_1) and HEX (H_1) → LAM (L_α). In the case of $PB_{202}E_{360}$ (PB−PEO-8) and $PB_{423}E_{484}$ (PB−PEO-11), the $I_1 \rightarrow H_1$ phase transition occurs at around $\phi_{PB} \approx 0.19$. There is a broad H_1/L_α coexistence region at $0.28 < \phi_{PB} < 0.36$ ($PB_{125}E_{155}$ (PB−PEO-14), $PB_{202}E_{360}$ (PB−PEO-8)). Above ϕ_{PB}, the lamellar phase is stable. One may compare the position of these phase transitions to those of pure block copolymer melts. According to Matsen et al.[41] phase transitions bcc (I_1) → HEX (H_1) and HEX (H_1) → LAM (L_α) occur at $\phi_{PB} = f_v = 0.117$ and 0.310, respectively. These values represent the strong segregation limit (SSL), which should be a good description of amphiphilic systems with high interfacial tension between hydrophilic and hydrophobic domains. We observe phase transitions in lyotropic phases to occur at higher volume fractions which indicates higher osmotic pressure in the solvent-swollen PEO matrix. A shift of the phase transitions to higher volume fractions corresponds to a decrease of the area per chain, $\bar{a}$, when going from spherical to cylindrical and lamellar geometry.

This is shown in Figure 11. The area per chain is taken from Table 2 and divided by the value for the spherical geometry. The low molecular weight block copolymer $PB_{125}E_{155}$ (PB−PEO-14) shows only a small decrease in going from spherical to cylindrical geometry. For the larger $PB_{202}E_{360}$ (PB−PEO-8), $PB_{432}E_{484}$ (PB−PEO-11), and $PB_{797}E_{893}$ (PB−PEO-12) the reduction becomes more pronounced. The area per chain reflects the influence of the anchored soluble chains as has been recently shown for the micellization of amphiphilic block copolymers.[73] The observed reduction of $\bar{a}$ thus corresponds to a de-swelling of the soluble polymer chains upon transitions into cylindrical and lamellar morphology with increasing polymer concentration. This effect seems to be more pronounced for high molecular weight polymers because of the larger contribution of the chain conformational entropy.

The dominance of an entropic contribution with increasing chain length is also apparent in the loss of order in the lyotropic phases. We observe with increasing molecular weight the tendency to form less ordered phase morphologies. $PB_{125}E_{155}$ (PB−PEO-14) forms large ordered domains. In the H_1/L_α coexistence region we observe well-defined domain boundaries whereas in the same coexistence region of $PB_{202}E_{360}$ (PB−PEO-8) cylinders and bilayers are almost homogeneously mixed. $PB_{202}E_{360}$ (PB−PEO-8) forms a well-ordered bcc cubic micellar phase (I_1), whereas $PB_{432}E_{484}$ (PB−PEO-11) only forms a disordered micellar phase (L_1). Similarly, the H_1 domains of $PB_{202}E_{360}$ (PB−PEO-8) are well ordered in contrast to $PB_{432}E_{484}$ (PB−PEO-11) where only in small domains cylinders pack hexagonally whereas in most regions cylinders form a transient network. $PB_{797}E_{893}$ (PB−PEO-12) shows the coexistence of spherical and wormlike micelles as well as vesicles in dilute solution. The size of the vesicles is quite small, indicating the effect of entropy, which favors the formation of the smallest association structures that are allowed by packing constraints. At a larger volume fraction, this polymer develops the highly disordered L_3 phase. Even at large volume fractions, in the range of the L_α phase, the degree of order is quite low.

From Table 2, we observe that well-ordered phases form above an interfacial area of $A_V^* = 0.02$ nm^{-1} per unit volume or a screening length of $\xi = 1/A_V^* = 50$ nm. Increasing the polymer chain length or adding solvent may lower the interfacial area per chain below this value and the phase disorders. Ordering is mediated by repulsive interactions of the soluble polymer chains. If the chains become sufficiently long or if solvent is added, the effect of the interface is screened and domains become less correlated. For very long polymer chains, the morphologies might be imagined to be similar to polymer blends that are compatibilized by block copolymers.[74] A further effect which suppresses ordering for high molecular weight entangled block copolymers is slow ordering kinetics, which prevents the formation of ordered structures within a typical experiment time.

Block copolymer lyotropic phases have recently attracted attention because of the possibility to prepare mesoporous inorganic structures that have pore diameters in the range 2−50 nm.[75,76] These materials are potentially useful as solid substrates in catalysis and chromatography.[77] They possess large specific surface areas that can be calculated as

$$A_{\mathrm{sp}} = \frac{d\phi}{(1-\phi)R\rho_{\mathrm{SiO_2}}} \tag{7}$$

where ρ is the density of the material. Taking, $\rho_{\mathrm{SiO_2}} = 2.1$ g/cm^3 for SiO_2, $d = 2$ for the H_1 phase, and $\phi = {}^1/_2$, one covers a range of $1905 \geq A_{\mathrm{sp}} \geq 38$ m^2/g of specific surface area in the mesoporous size range ($1 \leq R \leq 25$ nm).

The porous materials are generated via a sol/gel process that solidifies the aqueous domain of the lyotropic phase, followed by calcination to remove the polymer to leave a porous inorganic structure. In a previous paper we demonstrated that the porous domains are exact templates of the hydrophobic domains of the lyotropic phase.[21] Templating a γ-ray cross-linked and a non-cross-linked H_1 phase of $PB_{125}E_{155}$ (PB−PEO-14) resulted in the same mesoporous silicate structure. The diameter of the cylindrical H_1-pores ($2R_{cyl} = 27$ nm) was in good agreement with the diameter of the cylindrical PB domains in the H_1 phase ($2R_{cyl} = 26$ nm, Table 2). Silicate structures that are casts of lyotropic phases obtained from $PB_{432}E_{484}$ (PB−PEO-11) and $PB_{797}E_{893}$ (PB−PEO-12) have also been recently reported.[78] The unusual silicate templates observed for $PB_{797}E_{893}$ (PB−PEO-12) (Fig. 2 in ref 78) can now be attributed to the lyotropic L_3- and L_α-bilayer structures (Figure 8) that were used as their templates. An interesting point is the possibility to prepare stable lamellar or slit-pore structures from the defect-rich L_α phase of $PB_{797}E_{893}$ (PB−PEO-12) whereas such a structure expectedly collapsed for the well-ordered L_α phase of $PB_{432}E_{484}$ (PB−PEO-11). Defects such as bilayer bridges and cross-links act to mechanically stabilize porous lamellar domains. Also the $L_1 \rightarrow H_1 \rightarrow L_\alpha$ phase sequences observed for $PB_{125}E_{155}$ (PB−PEO-14) could be templated with a commercially available $PEE_{68}E_{66}$ (KLE−3729, Th. Goldschmidt) block copolymer.[79]

4. Conclusions

Poly(butadiene-*b*-ethylene oxide) copolymers are versatile model compounds to investigate lyotropic phase behavior of amphiphilic block copolymers. Lyotropic liquid crystalline phases of PB−PEO covering a degree of polymerization of $118 \leq N \leq 1690$ were investigated by scattering techniques (SAXS, SANS) and microscopy (TEM, POM). Cross-linking of lyotropic phases by γ-irradiation facilitated sample preparation and imaging by TEM. The medium molecular weight amphiphilic block polymers form type-1 lyotropic phases comprising disordered micellar solutions (L_1), spheres arranged on a bcc lattice (I_1), hexagonally packed cylinders (H_1), and lamellae (L_α). Increasing molecular weight destabilizes the I_1 and H_1 phase und suppresses the degree of order. For high molecular weight amphiphilic block copolymers, we observe the formation of the sponge phase (L_3). The transmission electron micrographs allow a detailed analysis of epitaxial relations, packing defects and their relation to optical textures.

Acknowledgment. We thank M. Dreja and B. Tiecke (University of Cologne) for the γ-ray cross-linking, R. Pitschke for support with TEM sample preparation, and K. Zenke for SAXS measurements. Financial support by the Deutsche Forschungsgemeinschaft (SFB 1623, A5), the Max-Planck-Gesellschaft, and the Dr.-Hermann-Schnell Foundation is gratefully acknowledged.

References and Notes

(1) Riess, G.; Hurtrez, G.; Bahadur, P. In *Encyclopedia of Polymer Science and Engineering*; Mark, H. F., Bikales, N. M., Overberger, C. G., Menges, G., Eds.; Wiley: New York, 1985.
(2) Edens, M. W. In *Nonionic Surfactants: Polyoxyalkylene Block Copolymers*, Nace, V. M., Ed.; Marcel Dekker Inc.: New York, 1996.
(3) Förster, S.; Antonietti, M. *Adv. Mater.* **1998**, *10*, 195.
(4) Schmolka, I. R.; Bacon, L. R. *J. Am. Oil Chem. Soc.* **1967**, *44*, 559.
(5) Chu, B.; Zhou, Z. In *Nonionic Surfactants: Polyolyalkylene Block Copolymers*; Nace, V. M., Ed.; Marcel Dekker: New York, 1996; Vol. 60, p 67.
(6) Mortensen, K. *J. Phys.: Condens. Matter* **1996**, *8*, A103.
(7) Alexandridis, P. *Curr. Opin. Colloid Interface Sci.* **1997**, *2*, 478.
(8) Schmolka, I. R. In *Nonionic Surfactants*; Schick, M. J. Ed.; Surfactant Science Series 1; Marcel Dekker: New York, 1967.
(9) Sun, W.-B.; Ding, J.-F.; Mobbs, R. H.; Attwood, D.; Booth, C. *Colloids Surf.* **1991**, *54*, 103.
(10) Luo, Y.-Z.; Nicholas, C. V.; Attwood, D.; Collett, J. H.; Price, C.; Booth, C. *Colloid Polym. Sci.* **1992**, *270*, 1094.
(11) Wanka, G.; Hoffmann, H.; Ulbricht, W. *Macromolecules* **1994**, *27*, 4145.
(12) Zhang, K.; Khan, A. *Macromolecules* **1995**, *28*, 3807.
(13) Alexandridis, P.; Zhou, D.; Khan, A. *Langmuir* **1996**, *12*, 2690.
(14) Svensson, M.; Alexandridis, P.; Linse, P. *Macromolecules* **1999**, *32*, 637.
(15) Bedells, A. D.; Arafeh, R. M.; Yang, Z.; Attwood, D.; Heatley, F.; Padget, J. C.; Price, C.; Booth, C. *J. Chem. Soc., Faraday Trans.* **1993**, *89*, 1235.
(16) Esswein, B.; Möller, M. *Angew. Chem., Int. Ed. Engl.* **1996**, *35*, 623.
(17) Hillmyer, M. A.; Bates, F. S. *Macromolecules* **1996**, *29*, 6994.
(18) Allgaier, J.; Poppe, A.; Willner, L.; Richter, D. *Macromolecules* **1997**, *30*, 1582.
(19) Förster, S.; Krämer, E. *Macromolecules*, **1999**, *32*, 2783.
(20) Hajduk, D. A.; Kossuth, M. B.; Hillmyer, M. A.; Bates, F. S. *J. Phys. Chem. B* **1998**, *102*, 4269.
(21) Hentze, H.-P.; Krämer, E.; Berton, B.; Förster, S.; Antonietti, M. *Macromolecules* **1999**, *32*, 5803.
(22) Lindner, P. In *Modern Aspects of Small-Angle Scattering*; Brumberger, E., Ed.; NATO Advanced Study Institutes, Series C.; Kluwer Academic: London, 1993; Vol. 451.
(23) Hoffmann, H. *Ber. Bunsen-Ges. Phys. Chem.* **1994**, *98*, 1433.
(24) Almgren, M.; Edwards, K.; Gustafsson, J. *Curr. Opin. Colloid Interface Sci.* **1996**, *1*, 270.
(25) Thurmond, K. B.; Kowalewski, T.; Wooley, K. L. *J. Am. Chem. Soc.* **1996**, *118*, 7239.
(26) Yang, J. L.; Wegner, G. *Macromolecules* **1992**, *25*, 1791.
(27) Guo, A.; Liu, G.; Tao, J. *Macromolecules* **1996**, *29*, 2487.
(28) Liu, G.; Qiao, L.; Guo, A. *Macromolecules* **1996**, *29*, 5508.
(29) Liu, G. *Curr. Opin. Colloid Interface Sci.* **1998**, *3*, 200.
(30) Won, Y.-Y.; Davis, H. T.; Bates, F. S. *Science* **1999**, *283*, 960.
(31) McGinniss, V. D. In *Encyclopedia of Polymer Science and Engineering* Mark, H. F., Bikales, N. M., Overberger, C. G., Menges, G., Eds.; Wiley: New York, 1985.
(32) Flory, P. J. *Principles of Polymer Chemistry*; Cornell University Press: Ithaca, NY, 1953.
(33) Fetters, L. J.; Lohse, D. J.; Richter, D.; Witten, T. A. *Macromolecules* **1994**, *27*, 4639.
(34) Smith, G. D.; Yoon, D. Y.; Jaffe, R. L.; Colby, R. H.; Krishnamoorti, R.; Fetters, L. J. *Macromolecules* **1996**, *29*, 3462.
(35) Mitchell, D. J.; Tiddy, G. J. T.; Waring, L.; Bostock, T.; McDonald, M. P. *J. Chem. Soc., Faraday Trans.* **1983**, *79*, 975.
(36) Seddon, J. *Biochim. Biophys. Acta* **1990**, *41*, 525.
(37) Buitenhuis, J.; Förster, S. *J. Chem. Phys.* **1997**, *107*, 262.
(38) McConnell, G. A.; Gast, A. P.; Huang, J. S.; Smith, S. D. *Phys. Rev. Lett.* **1993**, *31*, 6958.
(39) Robbins, M. O.; Kremer, K.; Grest, G. S. *J. Chem. Phys.* **1988**, *88*, 3286.
(40) Monovoukas, Y.; Gast, A. P. *J. Colloid Interface Sci.* **1989**, *128*, 533.
(41) Matsen, M. W.; Bates, F. S. *Macromolecules* **1996**, *29*, 1091.
(42) Israelachvili, J. N.; Mitchell, D. J.; Ninham, B. W. *J. Chem. Soc., Faraday Trans. 2* **1976**, *72*, 1525.
(43) Cates, M. E.; Candau, S. J. *J. Phys.: Condens. Matter* **1990**, *2*, 6869.
(44) Mortensen, K.; Talmon, Y.; Gao, B.; Kopps, J. *Macromolecules* **1997**, *30*, 6764.
(45) De Gennes, P. G. *Scaling Concepts in Polymer Physics*; Cornell University Press: Ithaca, NY, 1979.
(46) Schurtenberger, P.; Cavaco, C.; Tiberg, F.; Regev, O. *Langmuir* **1996**, *12*, 2894.
(47) Mortensen, K. *Curr. Opin. Colloid Interface Sci.* **1998**, *3*, 12.
(48) Wang, W.; Hashimoto, T. *Macromolecules* **1999**, *32*, 3163.
(49) Yang, J.; Wegner, G. *Macromolecules* **1992**, *25*, 1786.

(50) Boden, N. In *Micelles, Membranes, Microemulsions, and Monolayers*; Gelbart, W. M., Ben-Shaul, A., Roux, D., Eds.; Springer, New York, 1994.
(51) Gido, S. P.; Gunther, J.; Thomas, E. L. *Macromolecules* **1993**, *26*, 4506.
(52) Boltenhagen, P.; Lavrentovich, O.; Kleman, M. *Phys. Rev. A* **1992**, *46*, R1743.
(53) Zipfel, J.; Lindner, P.; Tsianou, M.; Alexandridis, P.; Richtering, W. *Langmuir* **1999**, *15*, 2599.
(54) Hillmyer, M. A.; Bates, F. S.; Almdal, K.; Mortensen, K.; Ryan, A. J.; Fairclough, J. P. A. *Science* **1996**, *271*, 976.
(55) Porte, G.; Marignan, J.; Bassereau, P.; May, R. *J. Phys.* **1988**, *49*, 511.
(56) Gazeau, D.; Bellocq, A. M.; Roux, D.; Zemb, T. *Europhys. Lett.* **1989**, *9*, 447.
(57) Strey, R.; Jahn, W.; Porte, G.; Bassereau, P. *Langmuir* **1990**, *6*, 1635.
(58) Munkert, U.; Hoffmann, H.; Thunig, C.; Meyer, H. W.; Richter, W. *Prog. Colloid Polym. Sci.* **1993**, *93*, 137.
(59) Alibert, I.; Coulon, C.; Bellocq, A. M.; Gulik-Krzywicki, T. *Europhys. Lett.* **1997**, *39*, 563.
(60) Hecht, E.; Mortensen, K.; Hoffmann, H. *Macromolecules* **1995**, *28*, 5465.
(61) Bates, F. S.; Maurer, W. M.; Lipic, P. M.; Hillmyer, M. A.; Almdal, K.; Mortensen, K.; Fredrickson, G. H.; Lodge, T. P. *Phys. Rev. Lett.* **1997**, *79*, 849.
(62) Hillmyer, M. A.; Maurer, W. W.; Lodge, T. P.; Bates, F. S.; Almdal, K. *J. Phys. Chem. B* **1999**, *103*, 4814.
(63) Vinches, C.; Coulon, C.; Roux, D. *J. Phys. II* **1994**, *4*, 1165.
(64) Filali, M.; Porte, G.; Appell, J.; Pfeuty, P. *J. Phys. II* **1994**, *4*, 349.
(65) Filali, M.; Appell, J.; Porte, G. *J. Phys. II* **1995**, *5*, 657.
(66) Patrick, H. N.; Warr, G. G.; Manne, S.; Aksay, I. A. *Langmuir* **1997**, *13*, 4349.
(67) Semenov, A. N. *Macromolecules* **1993**, *26*, 6617.
(68) Derici, L.; Ledger, S.; Mai, S.-M.; Booth, C.; Hamley, I. W.; Pedersen, J. S. *Phys. Chem. Chem. Phys.* **1999**, *1*, 2773.
(69) Mortensen, K.; Brown, W.; Jorgensen, E. B. *Macromolecules* **1995**, *28*, 1458.
(70) Hamley, I. W.; Pople, J. A.; Ameri, M.; Attwood, D.; Booth, C.; Ryan, A. J. *Macromol. Chem. Phys.* **1998**, *199*, 1753.
(71) Hamley, I. W.; Pople, J. A.; Ameri, M.; Attwood, D.; Booth, C. *Colloids Surf. A* **1998**, *145*, 185.
(72) Alexandridis, P.; Spontak, R. J. *Curr. Opin. Colloid Interface Sci.* **1999**, *4*, 130.
(73) Förster, S.; Zisenis, M.; Wenz, E.; Antonietti, M. *J. Chem. Phys.* **1996**, *104*, 9956.
(74) Macosko, C. W.; Guegan, P.; Khandpur, A. K.; Nakayama, A.; Marechal, P.; Inoue, T. *Macromolecules* **1996**, *29*, 5590.
(75) Göltner, C. G.; Henke, S.; Wei*β*enberger, M. C.; Antonietti, M. *Angew. Chem.* **1998**, *110*, 633.
(76) Krämer, E.; Förster, S.; Göltner, C. G.; Antonietti, M. *Langmuir* **1998**, *14*, 2027.
(77) Ying, J. Y.; Mehnert, C. P.; Wong, M. S. *Angew. Chem.* **1999**, *38*, 59.
(78) Göltner, C. G.; Berton, B.; Krämer, E.; Antonietti, M. *Adv. Mater.* **1999**, *11*, 395.
(79) Göltner, C. G.; Berton, B.; Krämer, E.; Antonietti, M. *Chem. Commun.* **1998**, 2287.

MA001923H